# High-temperature thermoelectric properties of *n*-type PbSe doped with Ga, In, and Pb

John Androulakis and Yeseul Lee
*Department of Chemistry, Northwestern University, Evanston, Illinois 60208, USA*

Iliya Todorov and Duck-Young Chung
*Materials Science Division, Argonne National Laboratory, Argonne, Illinois 60439, USA*

Mercouri Kanatzidis*
*Department of Chemistry, Northwestern University, Evanston, Illinois 60208, USA*
*Materials Science Division, Argonne National Laboratory, Argonne, Illinois 60439, USA*
(Received 24 January 2011; revised manuscript received 15 April 2011; published 31 May 2011)

We report a systematic study of the thermoelectric properties of PbSe doped with Ga, In, and excess Pb as a function of carrier density and temperature. All metal dopants efficiently generate electron carriers in the crystal lattice with densities as high as $\sim 10^{20}$ cm$^{-3}$ measured by the Hall effect. The Seebeck coefficient as a function of carrier density at room temperature was found to be similar for all dopants, while at 700 K substantial differences were observed with PbSe-In exhibiting a larger response. Infrared spectral reflectivity measurements at room temperature showed that both Ga and In substitution in PbSe weakens the curvature of the dispersion relation of the conduction band compared to Pb. This electronic effect contributes a larger density of states in transport processes at high temperatures. We have obtained thermoelectric figures of merit of $\sim$0.9 at 900 K, exceeding that of PbTe for $T > 800$ K.

DOI: 10.1103/PhysRevB.83.195209 PACS number(s): 72.20.Pa, 71.20.Nr

## I. INTRODUCTION

The rocksalt-structured, narrow-band-gap, lead-chalcogenide semiconductors (PbQ, Q = S, Se, Te) continue to attract considerable scientific interest[1–3] and have found several applications such as infrared photoresistors, photodiodes, lasers, and strain gauges.[4] In the past two decades, however, the global awakening for more efficient energy management has focused attention on the potential thermoelectric applications of these materials. Thermoelectricity refers to the conversion of heat into electrical energy by utilizing the Seebeck effect. A good candidate material should have the highest possible dimensionless figure of merit, $ZT = \frac{S^2\sigma T}{\kappa}$, where $S$ is the Seebeck coefficient, $\sigma$ the electrical conductivity, and $\kappa$ the thermal conductivity all measured at the same temperature, $T$. $ZT$ has no upper thermodynamic limit; however, most of the materials currently under consideration have a $ZT$ of $<2$.[5–8]

The study of thermoelectric energy conversion in lead chalcogenides has mainly focused on PbTe,[5,6] which is limited to $\sim$800 K. The selenium analog, PbSe, can potentially play a significant role in the advancement of thermoelectrics at temperatures above 800 K for several reasons. The overall efficiency $\eta$ of a thermoelectric engine depends not only on $ZT$ but also on the temperature difference of operation. This is quantified by the relation

$$\eta = \frac{T_H - T_C}{T_H} \frac{\sqrt{1+ZT}-1}{\sqrt{1+ZT}+\frac{T_C}{T_H}}, \quad (1)$$

where $T_H$ and $T_C$ are the high and low temperatures of operation of the thermoelectric engine, respectively (the first fraction is the Carnot efficiency). It is evident that $\eta$ can be increased by application of higher temperature gradients. Since PbSe has a higher melting point (1355 K) than PbTe (1253 K), it can in principle sustain higher operation temperatures up to 1000 K. Therefore, very high temperature applications (e.g., >800 K), including solar thermal energy conversion, could benefit from the development of PbSe-based thermoelectric generators.[9] At present, there are only a few materials considered for applications above 800 K: e.g., *p*-type $Si_{80}Ge_{20}$ with a maximum $ZT = 0.6$ at 873 K;[10,11] nanostructured *p*-type $Si_{80}Ge_{20}$ with enhanced $ZT \sim 0.95$ around 1100 K;[12] *n*-type $La_{3-x}Te_4$ that can inherently be doped by controlling off-stoichiometry of the elements;[13] the intermetallic *p*-type $Yb_{14}MnSb_{11}$,[14] which has a $ZT$ of approximately 1 at 1200 K; and multifilled skutterudites with $ZT \sim 1.2$ at 800–850 K.[15,16] PbSe is also attractive for high temperatures because it exhibits a monotonically increasing Seebeck coefficient even up to at least 1000 K, has a favorable electronic structure similar to that of PbTe, and has a lower lattice thermal conductivity at room temperature compared to PbTe.[17,18] Finally, Se is less expensive and $\sim$50 times more abundant than Te in the Earth's crust.[19] The aforementioned attractive combination of properties has prompted us to study in detail the thermoelectric behavior of PbSe at high temperatures.

Compared to PbTe, the thermoelectric and transport properties of PbSe and its solid solutions have attracted only limited attention, despite reports of a promising $ZT \sim 0.6$ around 700 K.[4] Nemov *et al.* have studied the amphoteric doping action of Bi in PbSe by means of the Hall effect and concluded that only a small fraction of Bi enters anionic sites at high Bi concentrations.[20] Alekseeva *et al.* have studied the properties of *p*-type PbSe and samples with isovalent Cd and Mn ion substitution, respectively,[21] and have reported promising properties without, however, determining accurately the doping levels of their specimens.[21] PbSe doped with In has been studied at temperatures above 77 K and the results were explained in the framework of the formation of an impurity band $\sim$0.24 eV above the bottom of the

 

conduction band that leads to resonant scattering and Fermi-level pinning.[22,23] The effect of Tl substitution for Pb in PbSe has also been discussed in the same context of resonance levels.[24] Schlichting and Gobrecht studied the mobility of *n*- and *p*-type PbSe from 0.3 to 800 K and for carrier densities ranging from $10^{16}$ to $10^{20}$ $cm^{-3}$ by controlling the stoichiometry of Pb and Se.[25] It was concluded that phonon scattering dominates the temperature region of interest for thermoelectric applications.

In this work we report a systematic and comparative study of the high-temperature thermoelectric properties (electrical resistivity, thermoelectric power, and thermal conductivity) of *n*-type samples of PbSe obtained using Ga, In, and excess Pb as donors, focusing on compositions with $>1 \times 10^{19}$ electrons/$cm^3$, i.e., practical for thermoelectric applications. We also present infrared (IR) reflectivity results at room temperature on mechanically polished samples as a function of carrier doping. The latter allowed us to extract electric-susceptibility effective mass values and draw conclusions on the possible changes the different dopants introduce in the electronic structure of PbSe. Unlike previous reports, we show that the $ZT$ values reach 0.9 at $T \sim 900$ K, which is higher than optimized pristine PbTe and suggest that PbSe is a very promising system for high-temperature thermoelectric applications.

## II. EXPERIMENTAL DETAILS

$Pb_{1-x}M_xSe$ (M = In, Ga) and $Pb_{1+x}Se$ samples, hereafter referred to as PbSe:M $x$%, were prepared by mixing high-purity (>99.99%) metals inside silica tubes. The maximum $x$ value for Ga and In was 3% while for Pb we have used up to an excess of 2%. The tubes were subsequently evacuated to a base pressure of $10^{-4}$ torr, fused, and heated over a period of 16 h at 1393 K idled for 4 h and then cooled down to room temperature over 3 hours. We have observed that the mechanical properties of the resulting ingots for PbSe:Pb depend on its reaction with the silica tube walls. Therefore, for Pb-doped samples graphite crucibles and/or carbon coating of the silica tubes was employed to avoid surface cracks and defects that deteriorated ingot quality during processing.

Powder x-ray diffraction studies, performed with an INEL diffractometer equipped with Cu Ka radiation and a position-sensitive detector, showed no indication for a second phase within the resolution of the instrument. The diffractograms were indexed in the $Fm\bar{3}m$ space group. A NETZSCH LFA 457 Microflash instrument was used to determine the thermal diffusivity of coin-shaped samples with a typical diameter of 6.8–7.9 mm and thickness of ~2 mm. The thermal conductivity $\kappa$ was then calculated by the relation $\kappa = DC_p\rho$, where $D$ is the thermal diffusivity, $C_p$ is the heat capacity under constant pressure, and $\rho$ is the mass density of the specimens. The $C_p$ values, in units of J/g K, were approximated by the relation $0.171 + (2.65 \times 10^{-5})T$, where $T$ is the temperature.[26] The geometrical dimensions of the specimens and their masses were used to determine their mass density that typically was found to be in the range $7.9 \leqslant \rho \leqslant 8.14$ g/$cm^3$, i.e., a 2.5%–4% difference from the theoretical value 8.24 g/$cm^3$.

The electrical conductivity $\sigma$ and Seebeck coefficient $S$ were measured simultaneously under a helium atmosphere (~0.1 atm) from room temperature to ~700 K using a ULVAC-RIKO ZEM-3 system. Samples measured >700 K were protected with insulating ceramic coating to avoid evaporation of Se and/or Pb. Generally the coated samples gave repeatable thermoelectric properties with little or no thermal hysteresis with thermal cycling.

The Hall coefficient was measured in a homemade room-temperature apparatus utilizing an electromagnet able to generate magnetic fields up to 1.4 T. A 4-point Hall-bar geometry (with soldered In as the contacts) was employed on the same specimens used for thermoelectric measurements. A 100 mA current, provided by a Keithley 6220 source, was passed through the specimens while the field was varied from 0.5 to 1.25 T in increments of 0.25 T and the voltage was recorded at each step with a Keithley 2182 A nanovoltmeter. The field was subsequently reversed and the procedure repeated. The antisymmetric dependence on the magnetic field (half-difference of the recorded voltages) was used as the Hall voltage. The error of the Keithley 2182A nanovoltmeter is ±300 nV which accounts for less than 5% in the error of the Hall voltage for the highly doped samples ($> 6 \times 10^{19}$ $cm^{-3}$). The carrier densities $n$ at room temperature were extracted on the assumption of a single band and a Hall factor $A = 1$ which gives for the Hall coefficient $R_H = 1/ne$, where $e$ is the electron charge. Accordingly the Hall mobilities $\mu_H$ were calculated on the assumption that the electrical conductivity is dominated by free electrons and thus $\mu_H = \sigma/ne$.

The effective mass of the samples was determined from measurements of the infrared spectral reflectivity as a function of wavelength (4–30 $\mu$m). The reflectivity was recorded with a Nicolet 6700 FTIR spectrometer equipped with a Spectra-Tech spectral reflectometer. The cylindrical specimens used to determine the thermal diffusivity were mechanically polished and used in this study. Since mechanically polished surfaces are prone to increase the uncertainty of the results we have only analyzed samples that exhibit a similar contribution of the bound electrons within a range of 5%, which are actually the samples with the best polished surfaces.

## III. RESULTS AND DISCUSSION

### A. Electrical charge transport

The electrical conductivity data as a function of temperature for all samples PbSe:M (M = In, Ga, Pb) studied in this work are depicted in Figs. 1(a)–1(c). The conductivity values indicate that In, Ga, and Pb are efficient dopants for PbSe.

TABLE I. Dopant concentrations and corresponding carrier densities for PbSe:M, M / Ga, In, Pb at room temperature.

| PbSe:Ga | | PbSe:In | | PbSe:Pb | |
|---|---|---|---|---|---|
| $x$% | $n(10^{19}\,cm^{-3})$ | $x$% | $n(10^{19}\,cm^{-3})$ | $x$% | $n(10^{19}\,cm^{-3})$ |
| 0.3 | 1.3 | 0.3 | 2.2 | 0.3 | 0.9 |
| 0.5 | 2.3 | 0.5 | 3.0 | 0.5 | 1.7 |
| 1.0 | 6.2 | 0.7 | 4.5 | 1.5 | 4.5 |
| 1.5 | 7.2 | 1.5 | 6.7 | 2.0 | 7.0 |
| 2.0 | 13.0 | 3.0 | 8.0 | 1.0 | 9.0 |

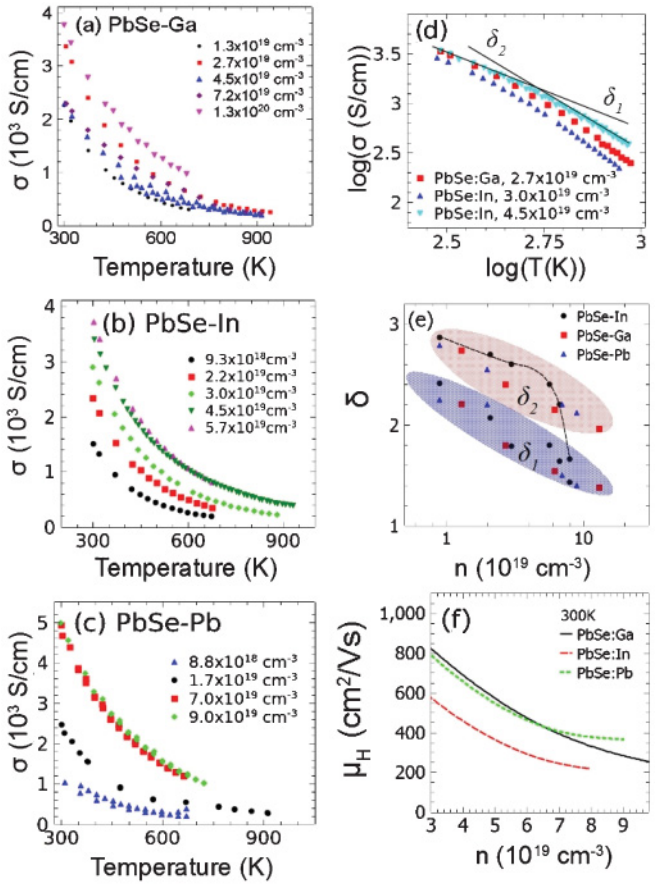


FIG. 1. (Color online) Electrical conductivity as a function of temperature and carrier density for (a) Ga-doped, (b) In-doped, and (c) Pb-doped PbSe. For clarity, we plot selected concentrations. (d) Examples of $\log\sigma - \log T$ plots that show two linear regions for which linear fits (black solid lines) yield $\delta$ exponents. The crossover region is ~450 K. (e) $\delta$ exponents as a function of carrier density. Two hatched regions are used to define the two linear regions that show up in $\log\sigma - \log T$ plots ($\delta_1$: linear fit results in the region 300 K $\leqslant T \leqslant$ 430 K, $\delta_2$: linear fit results in the region 460 K $\leqslant T \leqslant$ 700 K). The typical goodness of fit for each curve was >99%. Notice that for PbSe:In $\delta_2$ rapidly converges toward $\delta_1$ at high electron densities (the black dashed line is used as a guide to the eye). (f) Hall mobilities as a function of carrier concentration at room temperature. The Ga (black line) and Pb (green line) samples exhibit almost similar mobilities up to $\sim 6 \times 10^{19}$ cm$^{-3}$. For higher carrier densities Pb-doped samples have the highest mobilities compared to Ga and In doped. In-doped samples exhibit lower mobility for all $n$.

This is in agreement with Hall-effect measurements at room temperature that showed $n$-type character and electron densities in the range (1–10) $\times 10^{19}$ cm$^{-3}$. The carrier density was found to increase monotonically with Ga and In concentration. Pb-doping showed an anomalous behavior (see Table I), most probably because of the volatility of Se and the sensitivity of the crystal doping to defects created by Se vacancies.[25] Hence even a rough carrier density control with excess Pb was found to be challenging. The cast ingot nature of the samples makes them prone to microscale physical defects, grain boundaries, etc.

The decrease of $\sigma$ as a function of $T$ can be modeled by assuming an exponential dependence of the form $\sigma \sim T^{-\delta}$. The slope of a $\log\sigma - \log T$ plot, therefore, yields the exponent $\delta$. A single exponent cannot describe the data for all dopants. Rather, two linear regions, a low- and a high-temperature region, exist in the $\log\sigma - \log T$ plots requiring two exponents $\delta_1$ and $\delta_2$, respectively [see Fig. 1(d)]. Both $\delta_1$ and $\delta_2$ depend on the doping level and generally $\delta_2 > \delta_1$ while both exponents decrease with increasing doping. The results of the fittings are depicted in graphical form in Fig. 1(e). At low carrier densities, i.e., $<1 \times 10^{19}$ cm$^{-3}$ (dilute metal concentrations), PbSe exhibits a dopant independent behavior and therefore $\delta_1$ and $\delta_2$ have values close to 2.45 and 2.80, respectively. At high carrier densities the picture is very different for the In-doped samples where $\delta_1$ and $\delta_2$ are converging. Since the $\delta$ exponents are related to scattering mechanisms and the mobility, which in turn is related to band structure parameters, this behavior indicates considerable electronic structure differences in PbSe:In compared to PbSe:Pb.

Such a temperature dependence, i.e., decreasing slope of the temperature-dependent conductivity, is also present in PbTe where the results have been attributed to the effects of degeneracy in temperature and as a function of carrier density.[27] Therefore, we can assume that degeneracy sets in at a lower carrier density for PbSe:In than for PbSe:Ga and PbSe:Pb. We note that since the evolution from Boltzmann statistics to Fermi-Dirac statistics (i.e., when the electron gas becomes degenerate and therefore behaves like a metal) is smooth the transition temperature is defined somewhat arbitrarily. Pearson and Bardeen[28] defined the transition temperature $T_0$ as that when the energy of an electron (or hole) corresponding to the energy of a spherical Fermi surface is $k_B T_0$. In that case it holds that $T_0 \sim n^{2/3}$ and degeneracy dominates for $T \ll T_0$, while for $T \gg T_0$ the system is nondegenerate. Since the bands in lead chalcogenides around $\mathbf{k} = 0$ are nonparabolic the necessary conditions for degeneracy are more complex.[29]

Figure 1(f) presents room-temperature mobilities $\mu_H$ as a function of $n$. The PbSe:In system exhibits the lower mobility. On the other hand PbSe:Ga and PbSe:Pb have similar mobilities, within the error of the measurement, up to $\sim 6.5 \times 10^{19}$ cm$^{-3}$. At higher $n$ PbSe:Pb exhibits higher mobilities than the Ga and In systems. We note that despite using an excess of Pb, as high as 2%, a significant reduction in $\mu_H$ was not observed in PbSe:Pb. Such a feature can be explained as the result of Pb excess creating Se vacancies ($PbSe_{1-y}$), generating two carriers per atom without significantly altering the conduction band structure close to the Fermi level. Interestingly, Pb excess in PbTe acts in a completely different fashion since it precipitates out of the lattice forming inclusions that contribute to scattering and thus reduce the mobility by a factor of 3.[30] At the same time charge scattering by the inclusions were reported to contribute to an enhancement in the thermopower of the $Pb_{1+x}Te$ system.[30] This is yet another difference of excess Pb in PbSe compared to PbTe since we observed no such enhancements as will be discussed next.

The Seebeck coefficient for all metal dopants and selected doping levels as a function of $T$ is shown in Figs. 2(a)–2(c). The measurements were extended up to 900 K for the most promising compositions. A monotonic increase with no signs of saturation is observed for all carrier densities and metal

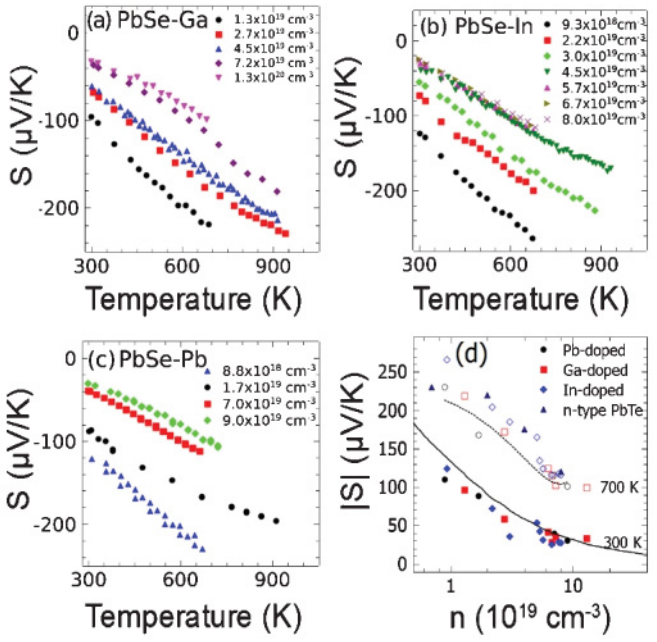


FIG. 2. (Color online) Seebeck coefficient as a function of temperature and carrier density for (a) Ga-doped, (b) In-doped, and (c) Pb-doped PbSe. In doping in PbSe generates a higher thermoelectric power in comparison to Ga and Pb dopants. (d) Pisarenko-type plots ($|S|$ vs carrier density) at 300 K (filled symbols) and 700 K for Pb-doped PbSe (dashed line), Ga-doped PbSe (open squares), and In-doped PbSe (open diamonds). The black solid line represents the theoretical prediction at room temperature taken from Ref. 30. Notice that at 700 K, In-doped samples show higher $S$ values compared to Pb-doped ones and essentially similar values to those of PbTe (blue filled up triangles).

dopants throughout the temperature range of the measurements, in sharp contrast to $n$-type PbTe[31] which exhibits bipolar diffusion effects above 800 K and thus its performance is deteriorated. Figure 2(d) presents Pisarenko plots,[32] i.e., thermopower vs carrier density, at two temperatures 300 K and 700 K, where filled and open symbols are used, respectively. The solid line at 300 K represents the theoretical prediction for PbSe as taken from Ref. 32 and it shows that all systems generally agree with the expected Seebeck coefficient response. The slight deviations from theory can be attributed to our assumption of parabolic bands and unitary Hall factor in the measurement of the carrier density. The solid blue triangles represent corresponding values of the thermopower at 700 K for the PbTe system doped with $PbI_2$ taken from Gelbstein *et al.*[31] The dotted black line is a fit of the 700 K thermopower data of the PbSe:Pb system.

Comparing the data in Fig. 2(d) we can conclude that (i) PbSe:In matches the thermopower output of PbTe at 700 K, and (ii) at carrier densities practical for thermoelectric applications PbSe:In exhibits the highest Seebeck coefficient followed by PbSe:Ga and finally PbSe:Pb. It is noteworthy that at high carrier densities all values converge. From these data it appears that PbSe has a great potential for thermoelectric applications at temperatures >700 K.

In order to gain further insight into the larger thermopower of the PbSe:In system compared to PbSe:Ga and PbSe:Pb we used Lorenz-Sommerfeld theory where the Seebeck coefficient of metals and degenerate semiconductors is related to $T$ with a simple formula that includes the density-of-states effective mass $m_d^*$ of the carriers: $S \sim \alpha m_d^* T n^{-2/3}$, where $\alpha$ is the constant of proportionality and $n$ is the carrier density.[33] Hall-effect measurements of $n$-type PbSe show that $n$ is almost constant at high temperatures[34] and therefore any differences in the Seebeck effect among the three types of dopants comes from $m_d^*$. A plot of the data as $S/T$ vs $T$ gives a representation of the dependence of $m_d^*$ with temperature. For the Ga samples we observe $m_d^*$ to be independent of $T$ for the entire doping range. Likewise the $S/T$ vs $T$ plot for the Pb-doped samples reveals only a weak dependence at higher carrier concentrations. In contrast the In-doped samples show a temperature-dependent $S/T$, almost linearly varying for the doping range $3 \times 10^{19}$ cm$^{-3} \leqslant n \leqslant 8 \times 10^{19}$ cm$^{-3}$. This indicates either a more complex scattering mechanism that enhances the average entropy per carrier or, more likely, a different temperature dependence of the electronic band structure at the Fermi level, that enhances the energy-dependent conductivity $\sigma(\varepsilon)$, which according to Mott's relation $S \sim \partial \ln \sigma(\varepsilon)/\partial \varepsilon$ enhances the thermopower.[35]

The only scattering mechanism considered for PbSe:In, other than electron-phonon scattering, is that of resonant scattering.[23] Such a mechanism should contribute to significant thermopower enhancements even at room temperature, but this is not observed in our data. Prokof'eva *et al.*[23] have made the same observation on PbSe:In codoped with Cl and concluded that resonant scattering is not present at higher temperatures. Generally, the effects of "resonant scattering" show up in the vicinity of liquid nitrogen temperatures rather than at or above room temperature.[23] In fact, the literature suggests that resonant scattering is likely not a practical mechanism to enhance the thermoelectric properties of semiconductors above cryogenic temperatures.[36] On the other hand recent results support resonant scattering as a thermopower-boosting process in Tl-doped PbTe especially at room temperature.[37] The apparent controversy is not yet resolved; however, based on the Pisarenko plot in Fig. 2(d) and a lack of carrier density pinning with increasing In concentration [see Table I and Fig. 1(f)] we conclude that resonant scattering is most probably not taking place at high temperatures and therefore the reasons for the enhancement in the thermopower of the PbSe:In system are related to band-structure effects.

Power factor (PF) values, i.e., $S^2\sigma$, for all three systems as a function of temperature are shown in Figs. 3(a)–3(c). It is readily seen that at 700 K the PFs have a tendency to converge between 10–15 $\mu$W/cmK$^2$. Samples with very high electrical conductivity, however, can exceed these values. For example, the PbSe:Ga sample with a carrier density of $2.7 \times 10^{19}$ cm$^{-3}$ exhibits a PF $\sim$ 17 $\mu$W/cmK$^2$ at 700 K which drops almost linearly to 13 $\mu$W/cmK$^2$ at 940 K. The overall power factor of all PbSe systems is lower than that of PbTe $\sim$ 700–750 K, by $\sim$3–6 $\mu$W/cmK$^2$.[31]

### B. Optical studies: Carrier effective mass determination

Useful information about the electronic band structure and transport properties of semiconductors can be obtained from spectral reflectivity measurements as a function of energy in

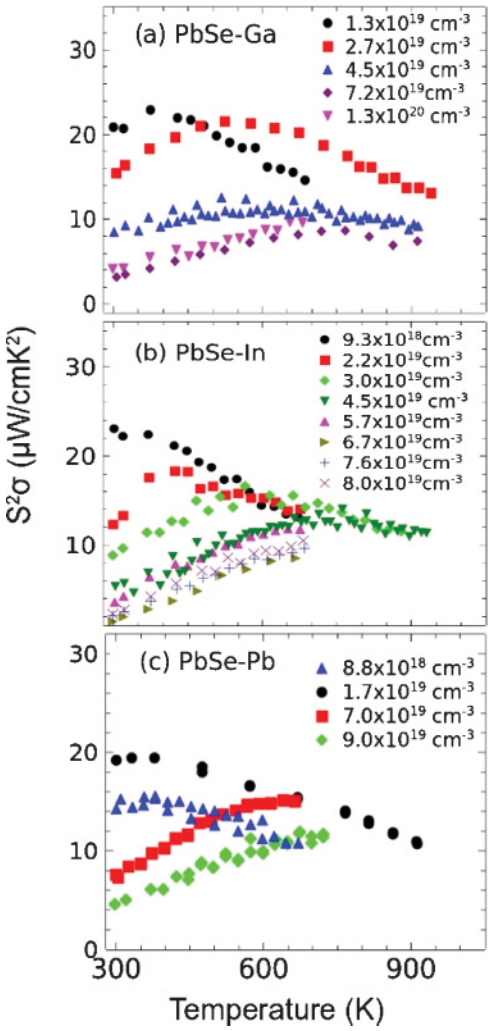


FIG. 3. (Color online) Corresponding power factors for (a) Ga-doped, (b) In-doped, and (c) Pb-doped PbSe. As a result of higher electrical conductivity the Ga- and Pb-doped samples exhibit higher values at 700 K.

the infrared part of the electromagnetic spectrum.[38] Generally the reflectivity $R$ depends on the contribution of bound and free electrons to the real part of the complex index of refraction $n_r$. The bound electron contribution shows up at low wavelengths $\lambda$, where $R$ should reach a constant value independent of carrier density. The free-electron contribution dominates at intermediate $\lambda$ values where $R$ reaches a minimum that depends strongly on the carrier density. Finally, at longer $\lambda$ values metallic reflection causes $R$ to assume uniformly high values. Figure 4(a) depicts representative spectra taken on In-doped samples and summarized in graphical form. $R$ can be expressed as a function of $n_r$ and $k_r$, the imaginary part of the complex refractive index, through the formula[38]

$$R = \frac{(n_r - 1)^2 + k_r^2}{(n_r + 1)^2 + k_r^2}. \tag{2}$$

In turn $n_r$ and $k_r$ are related to the real and imaginary parts of the dielectric function, $\varepsilon = \varepsilon_1 + i\varepsilon_2$, through the relations[38]

$$n_r = \frac{1}{\sqrt{2}}\left(\varepsilon_1 + \sqrt{\varepsilon_1^2 + \varepsilon_2^2}\right)^{1/2}, \tag{3}$$

$$k_r = \frac{1}{\sqrt{2}}\left(-\varepsilon_1 + \sqrt{\varepsilon_1^2 + \varepsilon_2^2}\right)^{1/2}. \tag{4}$$

Finally $\varepsilon_1$ and $\varepsilon_2$ are related to the optical dielectric constant $\varepsilon_\infty$, the plasma frequency $\omega_p$, and the energy independent scattering time $\tau = 1/\mu m^*$, where $m^*$ is the effective mass and $\mu$ the mobility of the carriers according to[38]

$$\varepsilon_1 = \varepsilon_\infty\left(1 - \frac{\omega_p^2\tau}{1 + \omega^2\tau^2}\right), \tag{5}$$

$$\varepsilon_1 = \frac{\varepsilon_\infty\omega_p^2\tau}{\omega(1 + \omega^2\tau^2)}. \tag{6}$$

Through an iterative fitting of $R$ to the above relations $m^*$ can be determined; see fit in the inset of Fig. 4(a). The derived optical effective masses of several of In-, Ga-, and Pb-doped PbSe specimens are presented in Fig. 4(b). The effective mass values seem to be higher than those previously reported in the literature for PbSe.[39] This may be the result of the strict parabolic bands model used in the analysis or the effect of a surface reconstruction that increases local ionicity of the bonds and thus excites the polarons. In general the polaron masses

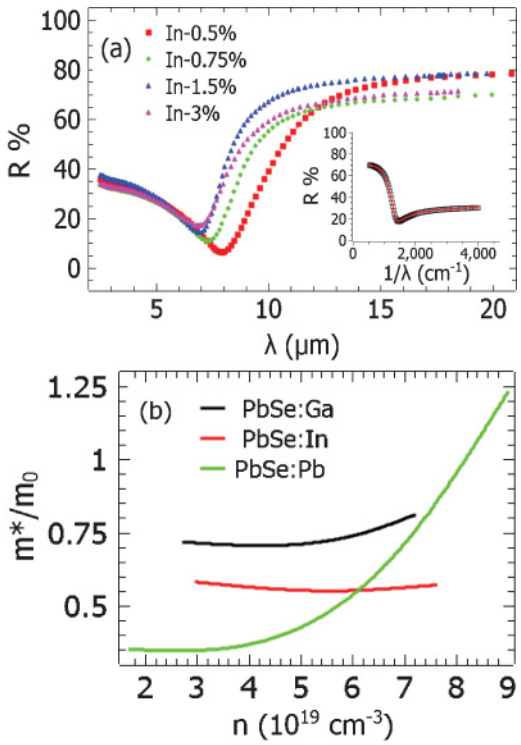


FIG. 4. (Color online) (a) Room-temperature infrared reflectivity spectra as a function of wavelength, $\lambda$, for In-doped PbSe. The $R$ minimum shifts to lower $\lambda$ with increasing In concentration indicative of the increase of the plasma frequency as a result of increasing carrier density. The inset shows a typical iterative analysis fit (red line) of the data (black circles) for the PbSe:In 1% sample. (b) Effective mass as a function of increasing $n$, for PbSe:Ga, PbSe:In, and PbSe:Pb. Notice that there is a strong dependence on $n$ for the Pb dopant as expected within the framework of ellipsoidal bands, a weaker one for Ga, and almost no dependence for In. This indicates that the dispersion relation of the conduction band is modified by the addition of Ga and In.

in Pb chalcogenides are of the order of one free-electron mass.[40] The fittings gave $\varepsilon_\infty$ values in the range 21–26 in reasonable agreement with those reported previously for PbSe, $\varepsilon_\infty = 23$.[41] For PbSe:Pb the effective mass seems to increase with increasing carrier density as expected for nonparabolic bands at the degenerate limit.[39] The same holds true for the PbSe:Ga samples, although the dependence is weaker. Interestingly, the effective mass of the PbSe:In system is relatively insensitive to the carrier density at room temperature.

A plausible explanation for the above observations consistent with our charge transport experimental results is as follows. Since PbSe is a narrow-band-gap semiconductor, Ga and In impurities in the lattice can hybridize with Pb $4s$ and Se $p$ orbitals and modify the band structure close to the Fermi energy. A measure of such changes can be provided by the dependence of the optical effective mass on carrier density. A large and continuous variation, as in the case of Pb doping, indicates that the energy bands involved are nonparabolic.[42] A linear combination of an ellipsoidal Fermi surface with a spherical one results in a less pronounced carrier dependence of the effective mass compared to a Kane-type model band only.[42] Therefore, we may conclude that excess Pb retains the characteristics of the band structure of PbSe, while Ga and In reduce the curvature of the dispersion of the conduction band close to the Fermi level, bringing the Fermi surface closer to a spherical shape. This, in turn, can affect the transport behavior of PbSe:In which shows an early onset of degeneracy, i.e., at lower carrier densities, as derived from the analysis of $\sigma(T)$ measurements (see previous section). The effect is weaker for Ga. A crude estimation of the proposed scheme on the density of states can be considered by taking into account the ratio of the density of states between the two extremes, i.e., an isotropic dispersion relation yielding a spherical Fermi surface and an anisotropic dispersion relation yielding and ellipsoidal Fermi surface. The difference between the density of states, $g(\varepsilon)$, that the two models yield shows up in the prefactor of $g(\varepsilon)$ that contains the effective mass.[43] The $g(\varepsilon)$ ratio of the two models is

$$\frac{g_{\rm iso}(\varepsilon)}{g_{\rm aniso}(\varepsilon)} \sim \frac{(m^*)^{3/2}}{(m_d^*)^{1/2}}, \tag{7}$$

where $m^*$ is a single-value effective mass and $m_d^* = (m_x m_y m_z)^{1/3}$ is the density-of-states effective mass. Therefore, we expect a slightly increased density of states in the case of a spherical Fermi surface and in the limit of low $\varepsilon$ usually involved in charge transport. From these considerations, a broadening of the distribution function with increasing temperature can potentially accommodate a larger density of states for PbSe:Ga and PbSe:In compared to Pb and result in increased thermoelectric power, a fact that correlates with the $S(T)$ results discussed above.

A schematic representation of the proposed picture of the DOS is depicted in Fig. 5. The dashed black line corresponds to the DOS of a parabolic isotropic dispersion relation while the solid black line corresponds to a parabolic anisotropic dispersion relation. At low energy values the difference in the curves is negligible; hence, the Fermi distribution function at 300 K accommodates the same DOS and therefore thermopower differences are negligible. At 700 K the isotropic DOS line lies higher and thus thermopower differences are

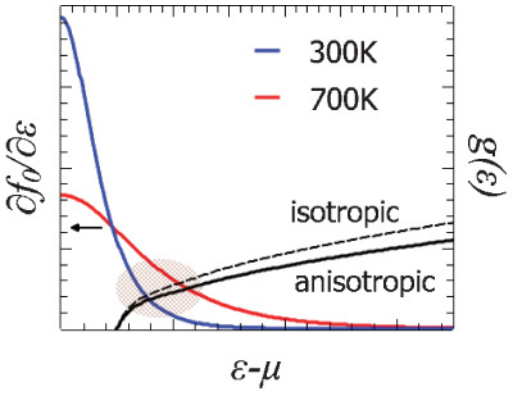


FIG. 5. (Color online) Schematic representation of the derivative of the Fermi distribution function, $\partial f_0/\partial\varepsilon$, and the density of states, $g(\varepsilon)$, of a hypothetical parabolic isotropic (dashed line) and parabolic anisotropic (solid black line) conduction band as a function of energy ($\mu$ is the chemical potential). The broadening of the Fermi distribution function as the temperature is increased from 300 K to 700 K accommodates a larger DOS for the isotropic, i.e., weaker dispersion, band.

measurable. Of course, a detailed experimental description of the dispersion relation with In and Ga substitution for Pb cannot be provided by this study. Furthermore, our infrared reflectivity analysis model is primarily based on parabolic dispersion assumptions. A more accurate analysis should take into account the prolate-ellipsoidal bands of PbSe along the $L$ point of the Brillouin zone.[39] Nevertheless, the above simple arguments are sufficient to capture essential differences between the density of states of PbSe:Pb and PbSe:(Ga, In) and give us a measure of insight in explaining the observed charge transport effects.

### C. Thermal conductivity

Figures 6(a)–6(c) depict the total thermal conductivity $\kappa$ as a function of temperature for all three sample systems. The values of $\kappa$ increase with increasing $n$ reflecting heat carried by free electrons. Values as high as 6 W/mK are observed at room temperature for PbSe:Pb with $9.0 \times 10^{19}$ cm$^{-3}$, 4.6 W/mK for PbSe:Ga with $7.0 \times 10^{19}$ cm$^{-3}$, and 3.8 W/mK for PbSe:In with $5.7 \times 10^{19}$ cm$^{-3}$. As expected, $\kappa$ decreases with increasing $T$ as a result of disturbances of the periodic potential of the lattice that increase the amplitude of phonon-phonon and electron-phonon scattering. The functional dependence of the decrease depends on carrier density for all three systems. For $n \sim 10^{18}$ $\kappa$ drops as $\sim 1/T^p$ where $p \sim 0.8$–$0.9$. At higher carrier densities the drop is more drastic so the exponent $p$ is $\sim 1$ or higher especially for PbSe:Pb. Since the measured $\kappa$ is the sum of two components of thermal conduction (lattice and free electrons) identifying their temperature-dependent contributions is crucial in not only explaining the behavior of thermal conductivity but also in further improving PbSe as a thermoelectric. In the following we show that the lattice thermal conductivity of PbSe remains almost unaffected with doping and therefore the temperature dependence as measured in Fig. 6 is largely determined by the carrier concentration.

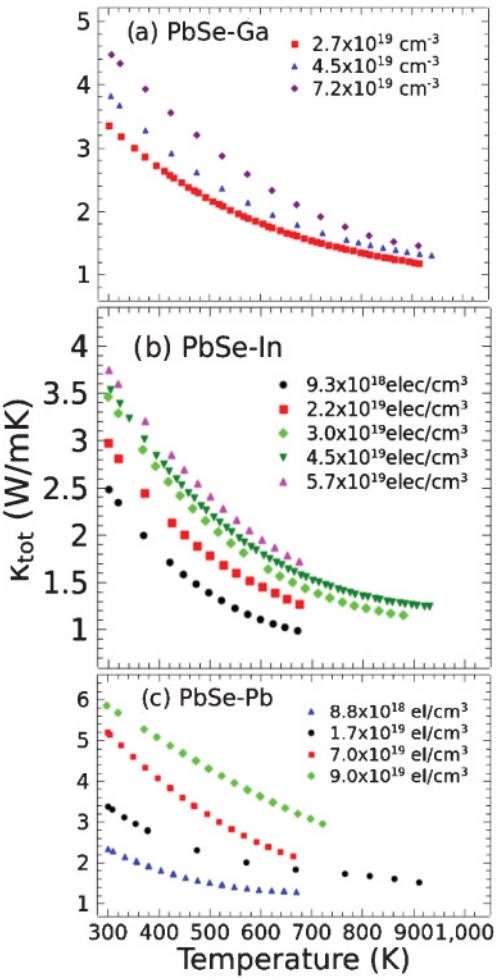


FIG. 6. (Color online) Thermal conductivities measured with the flash thermal diffusivity method for (a) Ga-doped, (b) In-doped, and (c) Pb-doped PbSe.

The electronic part of $\kappa$ is related to the mobility of carriers through the Wiedemann-Franz relation: $\kappa_e = L\sigma T$, where $L$ is a constant of proportionality called the Lorenz number. Although $L$ is usually assumed to take a universal value $L_0 = (\frac{\pi^2}{3})(\frac{k_B}{e})^2 \approx 2.44 \times 10^{-8}$ W K$^{-2}$ it is known that it is not the same for all materials[44] and can change significantly with temperature especially for semiconducting materials,[45] reflecting changes in chemical potential that bring the system outside of the limits of degeneracy. On the assumption of simple parabolic bands and a single predominant scattering mechanism, usually electron-phonon scattering, the Lorenz number can be expressed as a function of the chemical potential $\zeta$ according to

$$L = \frac{k_B^2}{e^2}\frac{3F_0(\zeta)F_2(\zeta) - 4F_1(\zeta)^2}{F_0(\zeta)^2}, \tag{8}$$

where $F_i$ is the appropriate order Fermi integral.[43,46] Since the Seebeck coefficient is also related to $\zeta$, then thermopower data can be fitted to extract $\zeta$ values at each temperature. Subsequently, $\zeta$ can be fed into Eq. (8) to yield the temperature dependence of $L$.[43,46] In the case of a predominant

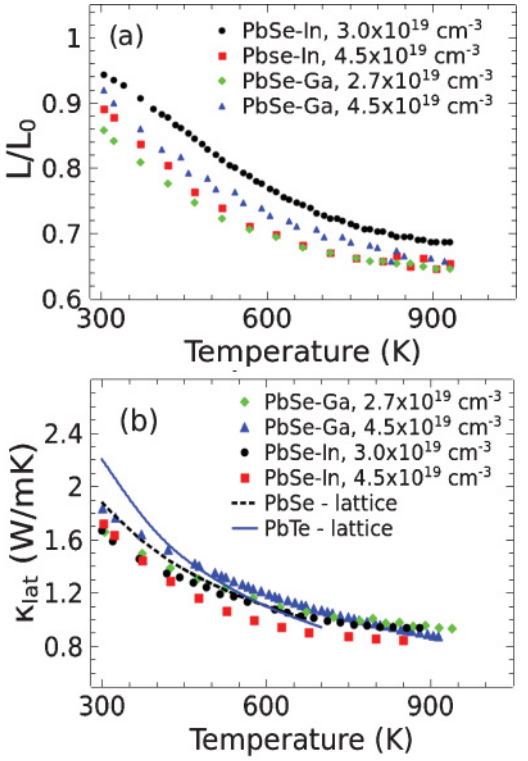


FIG. 7. (Color online) (a) Ratio of the Lorenz number $L$ calculated with Eq. (8) to the metallic value ($2.44 \times 10^{-8}$ W K$^{-2}$) as a function of temperature for doping levels in the range (2–5) $\times$ $10^{19}$ cm$^{-3}$ for Ga- and In-doped PbSe. (b) Lattice thermal conductivity plots as a function of temperature for PbSe:In and PbSe:Ga for similar doping level. The values were obtained after subtracting the electronic contribution from the total based on the Lorenz numbers of (a). The dashed black line is the measured thermal conductivity of a low carrier density ($< 2 \times 10^{18}$ cm$^{-3}$) PbSe crystal.

phonon-scattering mechanism the expression for the Seebeck coefficient is

$$S = \pm\frac{k_B}{e}\left(\frac{2F_1(\zeta)}{F_0(\zeta)} - \zeta\right). \tag{9}$$

Figure 7(a) depicts the results of this analysis for selected Ga and In samples, and shows a strong reduction of the Lorenz number at high temperature. The lattice part of the thermal conductivity can then be estimated by subtracting from the total measured $\kappa$ the electronic component $L\sigma T$, where both $L$ and $\sigma$ are temperature-dependent functions.

To directly determine the lattice thermal conductivity of pure PbSe we measured undoped samples so as to minimize the contribution of the free carriers. To this end, we have grown an undoped PbSe crystal in a Bridgman furnace setup. The crystal was measured to have a carrier density of $<2 \times 10^{18}$ cm$^{-3}$, ensuring that the electronic contribution to the thermal conductivity at room temperature would be <5%. This sample was measured up to 700 K and the data in the range 300 K $\leqslant T \leqslant$ 550 K were fitted to $1/T^p$ and extrapolated up to 700 K. This was necessary since thermal excitation of electron-hole pairs, the so-called bipolar diffusion,[47] in the conduction and valence bands above 600 K causes $\kappa$ to rapidly increase, which hinders the estimation of correct $\kappa_l$ values.

The dashed black line in Fig. 7(b) represents the measured and extrapolated lattice thermal conductivity of PbSe as a function of temperature. The line roughly follows a $\sim 1/T^{0.8}$ functional dependence. The results of the numerical analysis that allows the calculation of the lattice thermal conductivity of heavily doped samples, according to Eqs. (7) and (8), are included in Fig 7(b) for several specimens. The calculated lattice thermal conductivities are in good agreement with that of PbSe for samples with doping levels (1–5) $\times 10^{19}$ cm$^{-3}$. It is also evident that the calculated and measured values of thermal conductivity follow a similar power-law dependence. The lattice thermal conductivity of PbTe (blue solid line) as a function of temperature is also plotted for comparison on the same graph. Apparently, there is a different functional dependence of $\kappa_l$ on $T$ for the two compounds, with $\kappa_l^{\mathrm{PbTe}}$ decreasing faster than that of $\kappa_l^{\mathrm{PbSe}}$. Hence, although at room temperature $\kappa_l^{\mathrm{PbSe}} < \kappa_l^{\mathrm{PbTe}}$ the trend is reversed at 700 K, where PbTe has a lower lattice thermal conductivity by ~5%–6%.

This difference may be explained by the larger mean long wavelength acoustic mode Grüneisen parameter $\gamma$ in the high-temperature limit of PbSe compared to PbTe.[48] In general, increasing the Grüneisen parameter leads to anharmonicity and excitation of additional heat-carrying modes. A measure of the anharmonic contributions are given by the dimensionless quantity $\alpha\gamma T$, where $\alpha$ is the thermal expansion coefficient.[49] A reasonable assumption for the phononic mean free path $\ell_{\mathrm{ph}}$ is $\ell_{\mathrm{ph}} \approx A/\alpha\gamma$, where $A$ is the lattice spacing.[49] Taking into account that $\kappa_l \approx (1/3)C_v\ell_{\mathrm{ph}}\upsilon$, where $C_v$ the heat capacity under constant volume and $\upsilon$ is the sound velocity, and that for $T > 300$ K both compounds exhibit a similar $\alpha$,[50] one can calculate the ratio of $\kappa_l^{\mathrm{PbTe}}/\kappa_l^{\mathrm{PbSe}} \sim 1.03$ at 700 K on assuming the same sound velocity in the two compounds and that $C_v \approx C_p$. The heat capacity data were taken from Blachnik *et al.*[26] while the $\gamma$ values from Walker *et al.*[48] were used. The experimental value of the lattice thermal conductivity ratio of PbTe to PbSe at 700 K is 0.99. These simplistic arguments do not seem to lead in a prediction for a lower lattice thermal conductivity for PbTe at high temperatures. However, the agreement is reasonable and seems to explain the $\kappa_l^{\mathrm{PbTe}}/\kappa_l^{\mathrm{PbSe}}$ ratio reduction from 1.17 at 300 K to about 1 at 700 K. For completeness we mention that the same model predicts a room-temperature ratio of ~1.25.

The dimensionless figure of merit values derived from the measured data of Figs. 3 and 6 are shown in Figs. 8(a)–8(c) for each system. The solid black lines in Figs. 8(a) and 8(b) represent the $ZT$ of conventional optimized $n$-type PbTe that is included for comparison. For the PbSe:Pb system the rapidly falling PF with increasing temperature keeps the $ZT$ values low. On the other hand both Ga and In generate high $ZT$ values ~0.9 at 900 K. This value significantly exceeds that of $n$-type PbTe at 900 K which is ~0.63.[10,31] Therefore, according to Eq. (1), PbSe demonstrates greater conversion efficiency than PbTe in applications involving temperatures >800 K.

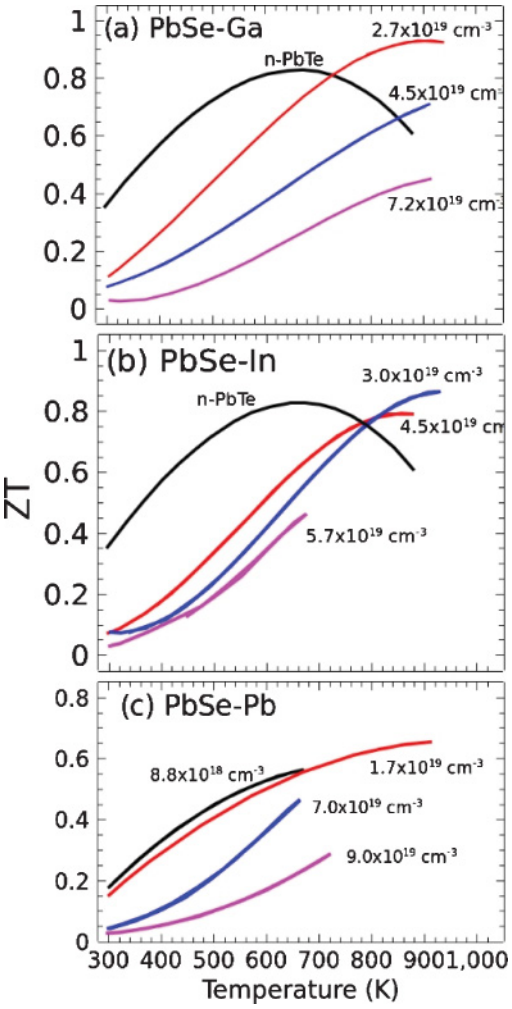


FIG. 8. (Color online) Dimensionless figures of merit ($ZT$) for different dopants (a) Ga, (b) In, and (c) Pb with a calculated uncertainty ±8% for (b) and ±12% for (a) and (c) and comparison with optimized $n$-type PbTe. Both Ga and In show a $ZT \sim 0.9$ at 900 K.

## IV. CONCLUSIONS

The thermoelectric properties of PbSe doped with Ga, In, and excess Pb investigated as a function of carrier density and temperatures up to 900 K indicate that degeneracy sets in at lower doping level for PbSe:In compared to Ga- and Pb-doped PbSe. Measurements of the effective mass as a function of doping at room temperature suggest that Pb doping retains the electronic structure of PbSe, while Ga and In distort the electronic density of states and decrease the curvature of the dispersion relation of the conduction band near the Fermi energy, the effect being stronger for In. The data, however, contain no evidence for resonance scattering at these high temperatures. We speculate, therefore, that the broadening of the electronic distribution function at high temperatures contributes to an increased thermoelectric power output for In compared to Ga and Pb. This electronic effect generates thermoelectric figures of merit $ZT \sim 0.9$ at 900 K for PbSe:Ga and PbSe:In (compared to only ~0.8 at 700 K and ~0.65 at 900 K for optimally doped PbTe).

There is a general perception in the reported literature that $n$-type PbTe is a significantly better thermoelectric material than PbSe at all temperatures. Our work in fact shows that the thermoelectric properties of these two systems are comparable at best at 800 K, and at 900 K PbSe actually outperforms

its tellurium analog. The significantly larger abundance of selenium compared to tellurium, coupled with the promising high-temperature thermoelectric results reported here, makes PbSe an attractive material system to focus on, with the aim of better understanding its fundamental properties and continuing to improve its performance. Our present work involved only the pristine PbSe material, and given the new paradigm of endotaxial nanostructuring as demonstrated in the PbTe-based materials,[6,51,52] we anticipate significant enhancements with continued development.

## ACKNOWLEDGMENTS

We thank Simon Johnsen for useful discussions and his help in the numerical calculations of the Lorenz numbers. This material is based on work supported as part of the Revolutionary Materials for Solid State Energy Conversion, an Energy Frontier Research Center funded by the US Department of Energy, Office of Science, Office of Basic Energy Sciences, under Award No. DE-SC0001054. The work at Argonne was supported by the US DOE, Office of Science, under Contract No. DE-AC02-06CH11357.

*m-kanatzidis@northwestern.edu

[1] E. S. Bozin, C. D. Malliakas, P. Souvatzis, T. Proffen, N. A. Spaldin, M. G. Kanatzidis, and S. J. L. Billinge, Science **330**, 1660 (2010).
[2] R. D. Schaller, S. A. Crooker, D. A. Bussian, J. M. Pietryga, J. Joo, and V. I. Klimov, Phys. Rev. Lett. **105**, 067403 (2010).
[3] J. J. H. Pijpers, R. Ulbricht, K. J. Tielrooij, A. Osherov, Y. Golan, C. Delerue, G. Allan, and M. Bonn, Nature Phys. **5**, 811 (2009).
[4] Y. I. Ravich, B. A. Efimova, and I. A. Smirnov, *Semiconducting Lead Chalcogenides*, edited by L. S. Stil'bans (Plenum Press, New York–London, 1970).
[5] J. R. Sootsman, D. Y. Chung, and M. G. Kanatzidis, Angew. Chem. Int. Ed. **48**, 8616 (2009).
[6] M. G. Kanatzidis, Chem. Mater. **22**, 648 (2010).
[7] C. Wan, Y. Wang, N. Wang, W. Norimatsu, M. Kusunoki, and K. Koumoto, Sci. Technol. Adv. Mater **11**, 044306 (2010).
[8] M. S. Dresselhaus, G. Chen, M. Y. Tang, R. G. Yang, H. Lee, D. Z. Wang, Z. F. Ren, J.-P. Fleurial, and P. Gogna, Adv. Mater. **19**, 1043 (2007).
[9] G. W. Crabtree and N. S. Lewis, Phys. Today **60**, 37 (2007).
[10] C. Wood, Energy Convers. Manage. **24**, 331 (1984).
[11] O. Yamashita and N. Sadatomi, J. Appl. Phys. **88**, 245 (2000).
[12] G. Joshi, H. Lee, Y. Lan, X. Wang, G. Zhu, D. Wang, R. W. Gould, D. C. Cuff, M. Y. Tang, M. S. Dresselhaus, G. Chen, and Z. Ren, Nano Lett. **8**, 4670 (2008).
[13] A. F. May, J. P. Fleurial, and G. J. Snyder, Phys. Rev. B **78**, 125205 (2008).
[14] S. R. Brown, S. M. Kauzlarich, F. Gascoin, and G. J. Snyder, Chem. Mater. **18**, 1873 (2006).
[15] G. Rogl, A. Grytsiv, P. Rogl, E. Bauer, M. B. Kerber, M. Zehetbauer, and S. Puchegger, Intermetallics **18**, 2435 (2010).
[16] Y. Z. Pei, J. Yang, L. D. Chen, W. Zhang, J. R. Salvador, and J. Yang, Appl. Phys. Lett. **95**, 042101 (2009).
[17] D. Parker and D. J. Singh, Phys. Rev. B **82**, 035204 (2010).
[18] T. Grandke, M. Cardona, and L. Ley, Solid State Commun. **32**, 353 (1979).
[19] Z. Hu and S. Gao, Chem. Geol. **253**, 205 (2008).
[20] S. A. Nemov, T. A. Gavrikova, V. A. Zykov, P. A. Osipov, and V. I. Proshin, Semiconductors **32**, 689 (1998).
[21] G. T. Alekseeva, E. A. Gurieva, P. P. Konstantinov, L. V. Prokof'eva, and M. I. Fedorov, Semiconductors **30**, 1125 (1996).
[22] V. I. Kaĭdanov, R. B. Mel'nik, and N. V. Germanas, Sov. Phys. Semicond. **6**, 627 (1972).
[23] L. V. Prokof'eva, E. A. Gurieva, Sh. M. Zhumaksanov, P. P. Konstantinov, Kh. R. Maĭlina, Yu. I. Ravich, and L. S. Stil'bans, Sov. Phys. Semicond. **21**, 1078 (1987).
[24] V. I. Kaĭdanov, S. A. Nemov, and Yu. I. Ravich, Sov. Phys. Semicond. **26**, 113 (1992).
[25] U. Schlichting and K. H. Gobrecht, J. Phys. Chem. Solids **34**, 753 (1973).
[26] R. Blachnik and R. Igel, Z. Naturforsch. B **29**, 625 (1974).
[27] A. F. Joffe and L. S. Stil'bans, Rep. Prog. Phys. **22**, 167 (1959).
[28] G. L. Pearson and J. Bardeen, Phys. Rev. **75**, 865 (1949).
[29] E. O. Kane, Phys. Rev. **131**, 79 (1963).
[30] J. P. Heremans, C. M. Thrush, and D. T. Morelli, J. Appl. Phys. **98**, 063703 (2005).
[31] Y. Gelbstein, Z. Dashevsky, and M. P. Dariel, Physica B **363**, 196 (2005).
[32] V. Jovovic, S. J. Thiagarajian, J. West, J. P. Heremans, T. Story, Z. Golacki, W. Paszkowicz, and V. Osinniy, J. Appl. Phys. **102**, 043707 (2007).
[33] G. J. Snyder and E. S. Toberer, Nature Mater. **7**, 105 (2008).
[34] E. Hirahara and M. Murakami, J. Phys. Soc. Jpn. **9**, 671 (1954).
[35] M. Jonson and G. D. Mahan, Phys. Rev. B **21**, 4223 (1980).
[36] Yu. I. Ravich, in *CRC Handbook of Thermoelectrics*, edited by D. M. Rowe (CRC Press, Boca Raton, 1995).
[37] J. P. Heremans, V. Jovovic, E. S. Toberer, A. Saramat, K. Kurosaki, A. Charoenphakdee, S. Yamanaka, and G. J. Snyder, Science **321**, 554 (2008).
[38] M. Fox, *Optical Properties of Solids* (Oxford University Press, Oxford, 2010).
[39] A. Aziza, E. Amzallag, and M. Balkanski, Solid State Commun. **8**, 873 (1970).
[40] R. Dalven, Phys. Rev. B **3**, 1953 (1971).
[41] D. Khokhlov, *Lead Chalcogenides* (Taylor and Francis, New York, 2003).
[42] J. R. Dixon and H. R. Riedl, Phys. Rev. **138**, A873 (1965).
[43] V. I. Fistul', *Heavily Doped Semiconductors* (Plenum Press, New York, 1969).
[44] C. Kittel, *Introduction to Solid State Physics* (John Wiley, New York, 1986).
[45] G. S. Kumar, G. Prasad, and R. O. Pohl, J. Mater. Sci. **28**, 4261 (1993).
[46] A. F. May, E. S. Toberer, A. Saramat, and G. J. Snyder, Phys. Rev. B **80**, 125205 (2009).
[47] J. Yang, in *Thermal Conductivity*, edited by T. M. Tritt (Springer, New York, 2004).
[48] N. J. Walker, G. A. Saunders, and N. Schäl, J. Phys. Chem. Solids **48**, 91 (1987).
[49] J. S. Dugdale and D. K. C. MacDonald, Phys. Rev. **98**, 1751 (1955).
[50] S. I. Novikova and N. Kh. Abrikosov, Sov. Phys. Solid State **5**, 1397 (1964).
[51] K. Biswas, J. He, Q. Zhang, G. Wang, C. Uher, V. P. Dravid, and M. G. Kanatzidis, Nature Chem. **3**, 160 (2011).
[52] S. Johnsen, J. Q. He, J. Androulakis *et al.*, J. Am. Chem. Soc. **133**, 3460 (2011).